



Nanoscale

**Ultra-stable blue-emitting lead-free double perovskite
Cs₂SnCl₆ nanocrystals enabled by an aqueous synthesis on
a microfluidic platform**

Journal:	<i>Nanoscale</i>
Manuscript ID	NR-ART-10-2022-005510
Article Type:	Paper
Date Submitted by the Author:	04-Oct-2022
Complete List of Authors:	Tang, Xiaobing; University of Kentucky, Chemical and Materials Engineering Wen, Xiyu; University of Kentucky Yang, Fuqian; University of Kentucky, Chemical and Materials Engineering

SCHOLARONE™
Manuscripts

ARTICLE

Ultra-stable blue-emitting lead-free double perovskite Cs₂SnCl₆ nanocrystals enabled by an aqueous synthesis on a microfluidic platform

Received 00th
January 20xx,
Accepted 00th
January 20xx

Xiaobing Tang,^a Xiyu Wen^b and Fuqian Yang^{a*}

DOI:
10.1039/x0xx00000x

Abstract

Blue emitting Sn-based lead-free halide perovskite nanocrystals (NCs) are considered to be a promising material in lighting and display. However, industrialised fabrication of blue-emitting NCs still remains a significant challenge due to the use of toxic solvent and optical instability, not mentioning in large-scale synthesis. In this work, a green-route synthesis of blue-emitting lead-free halide perovskite Cs₂SnCl₆ powders is developed, in which deionized water with small amount of inorganic acid is used as solvent and the synthesis of the Cs₂SnCl₆ powders is achieved by a microfluidic platform. Using the Cs₂SnCl₆ powders, we prepare Cs₂SnCl₆ NCs via an ultrasonication process. Changing the volume ratio of ligands (oleic acid to oleylamine) can alter the photoluminescence (PL) characteristics of the prepared NCs, including the PL-peak wavelength, PL-peak intensity and quantum yield. The highest photoluminescence quantum yield (PLQY) of 13.4% is achieved from the Cs₂SnCl₆ NCs made with 40 μL to 10 μL of the volume ratio of oleic acid to oleylamine. A long-term PL stability test demonstrates that the as-synthesized Cs₂SnCl₆ NCs can retain a stable PLQY over a period of 60 days. This work opens up a new path for large-scale green-route synthesis of blue-emitting Sn-based lead-free NCs, such as Cs₂SnX₆ (Cl, Br and I), towards the applications in optoelectronics.

Keywords: lead-free halide perovskite nanocrystals; green-route synthesis; Cs₂SnCl₆ nanocrystals.

^a Materials Program, Department of Chemical and Materials Engineering, University of Kentucky, Lexington, KY 40506, USA

^b Center for Aluminium Technology, University of Kentucky, Lexington, KY 40506, USA

*Corresponding author. E-mail: fuqian.yang@uky.edu (F. Yang)

Electronic Supplementary Information (ESI) available: [details of any supplementary information available should be included here]. See DOI: 10.1039/x0xx00000x

1. Introduction

Blue light, as an indispensable part of full-colour display, is of crucial importance in the area of lighting and display. Blue-emitting quantum dots (semiconductor nanocrystals (NCs)) have potential applications in optoelectronics, bioimaging and so forth, because they have a wide range of merits including high brightness, narrow full-width at half-maximum (FWHM) of photoluminescence (PL) spectrum, high colour purity, facile synthesis, etc. For the past few years, many efforts were focused on the synthesis of lead halide perovskite (LHP) NCs due to their high light absorption coefficient and high defect tolerance.¹⁻³ However, the reported blue LHP NCs exhibited severe agglomeration and caused a red shift of light emission in a short time, resulting in significant optical instability. For example, Bi et al.⁴ demonstrated that the PL-peak wavelength of blue-emitting CsPbBr₃ NCs changed from 470 nm to 500 nm in 12 min and the PL-peak wavelength of the modified NCs remained at 470 nm with a PL stability of only 1 h. Also, the toxic lead (Pb) element in the LHP NCs causes a concern for their large-scale applications and commercialization.

As an alternative, lead-free halide perovskite (LFHP) NCs are considered to be promising materials to replace the LHP NCs, among which, tin (Sn) (isovalent congener of lead)-based LFHP NCs have showed tremendous potential with decent optical characteristics and performance,^{5, 6} because compared with Pb-based perovskites, Sn-based perovskite counterparts have narrower bandgaps and higher charge mobilities.⁷ However, Sn-based perovskites have poor environmental stability, resulting from that partial Sn²⁺ can be easily oxidized to Sn⁴⁺.^{7, 8} The more air-stable Sn⁴⁺ introduces p-type self-doping effect and further lowers photophysical property of perovskites.⁷⁻⁹ Recently, several antioxidants were used to improve the stability of Sn-based perovskites and the corresponding devices.^{10, 11} However, improving the environmental stability of Sn-based LFHP NCs still remains challenges.

Several methods have been developed to synthesize blue-emitting Sn-based LFHP NCs. Hot injection (HI) is a favorable method for the synthesis of high-quality NCs with relatively uniform sizes. This method requires the synthesis under harsh conditions, including high temperature and vacuum for the formation of NCs.¹² Also, the HI approach uses toxic and volatile solvent, such as 1-octadecene (ODE), which impedes the industrialization of blue-emitting Sn-based LFHP NCs from a sustainable view. To address this issue, an aqueous-solution-based green synthesis route without the use of toxic solvent is a preferable choice. Tan et al.¹³ reported a solvothermal method for the synthesis of Bi-doped Cs₂SnCl₆ NCs with light emission at 455 nm. This method avoids the use of toxic solvent, while it requires the synthesis performed at a high temperature near 200 °C. It is also challenging to control the morphology and size of the prepared NCs due to that the formation of NCs was realized in a “random” cooling process from high temperature.¹³ It should be noted that all the methods mentioned above are suitable for small-scale synthesis of blue-emitting LFHP

NCs and may not be suitable for large-scale production to fulfill the industrialization and commercialization of blue-emitting Sn-based LFHP NCs.

Microfluidics has been demonstrated to be a reliable and powerful technique for large-scale manufacturing of nanoparticles and nanocrystals.¹⁴⁻¹⁶ Compared with the small-batch synthesis of materials of small volumes for fundamental research, microfluidics can provide continuous fabrication of materials and eliminate the samples' irreproducibility originating from batch-to-batch fabrication.¹⁷⁻¹⁹ Currently, microfluidics has been used to synthesize Pb-based NCs^{20, 21}. For example, Lignos et al.²⁰ produced all-inorganic perovskite CsPbX₃ (X = Cl, Br, I) NCs with the PL-peak wavelength ranging from 470 – 690 nm via microfluidics. Bao et al.²¹ incorporated microfluidics with inkjet printing technique to synthesize CsPbBr₃/Cs₄PbBr₆ nanocrystals for mini-LEDs. Recently, Xu et al. achieved large-scale synthesis of cesium lead halide perovskite NCs.^{22, 23} However, it still remains challenging to synthesize Sn-based LFHP NCs with an aqueous solution via a microfluidic platform.

Realizing the challenges faced in the synthesis of blue-emitting Sn-based LFHP NCs and the practical applications of blue-emitting Sn-based LFHP NCs in optoelectronics, we developed a green approach to produce blue-emitting Sn-based LFHP (Cs₂SnCl₆) NCs using a microfluidic platform and ultrasonication consecutively. The blue-emitting Cs₂SnCl₆ NCs exhibited a PL-peak wavelength centred at 435 nm with the highest PLQY of 13.4% and good long-term optical stability over a period of 60 days.

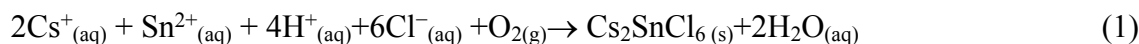
2. Experimental section

2.1 Materials

The chemicals used in this work were CsCl (99.9%, Alfa Aesar), SnCl₂ (Sigma Aldrich), oleylamine (OAm) (>50%, TCI America), oleic acid (OA) (Ward's Science), silicone elastomer base/curing agent, (Sylgard™ 184, Electron Microscopy Sciences), hexane (Sigma Aldrich), HCl acid (37%), toluene (VWR International LLC, 99.5%), isopropanol (IPA) (VWR International LLC, 99%), dichloromethane (BeanTown Chemical, 99.5%) and deionized (DI) water. No further purification was performed for all the received chemicals. HCl acid was diluted to 18.5% prior to use.

Cs₂SnCl₆ powder were first prepared. Specifically, 5 mmol CsCl powder and 5 mmol SnCl₂ powder were dissolved in 5 ml water and 5 ml HCl acid (18.5%), respectively, to produce a CsCl solution and a SnCl₂ solution. A microfluidics platform was assembled for the synthesis of Cs₂SnCl₆ powder at room temperature (Fig. 1). The CsCl solution and SnCl₂ solution were loaded in two syringes, respectively, which were placed on a Syringe Pump system (Harvard Apparatus). Both the CsCl solution (flow rate, 0.4 ml/min) and SnCl₂ solution (flow rate, 0.4 ml/min) were pumped into a microreactor through two capillaries (1.0 mm in inner diameter and 80 cm in length). These two solutions mixed and reacted in the microreactor to immediately form white products (precipitates). Note that all the procedures were carried out under ambient

conditions, in which Sn^{2+} is prone to be oxidized into Sn^{4+} . Equation 1 shows the chemical reaction taking place in the microreactor



The as-formed white precipitates flowed into another capillary tube (1.6 mm in inner diameter and 20 cm in length), which connected the microreactor to a container, for the collection of the white precipitates at a total flow rate of 0.8 ml/min. The collection of white precipitates by the microfluidics system is presented in Movie S1 in Supplementary Information, which shows that a white Cs_2SnCl_6 precipitate solution continuously flows through the capillary tube and to a small vial for the collection of the white Cs_2SnCl_6 precipitates, and demonstrates the feasibility of large-scale synthesis of the Cs_2SnCl_6 precipitates (powders). Moderate amounts of the white precipitates were put onto a glass plate at 30 °C for 1 h to achieve dry white powders. Using the microfluidic system, we were able to produce 0.06 g dry Cs_2SnCl_6 powders within 8 min (Fig. S1, Supplementary Information) with a production rate of 0.45 g/h. Note that this result reveals that the large-scale synthesis of Cs_2SnCl_6 perovskites by microfluidics is feasible and the production rate of 0.45 g/h is only for the microfluidics system used in this work.

A mixture of 5 mg of the white powders, 5 ml hexane and 50 μL ligands (mixture of OA and OAm) was placed in a 20 ml vial in a water bath, which was sonicated for 400 min at room temperature (RT). The solution with Cs_2SnCl_6 NCs was obtained by collecting the supernatant of the solution after ultrasonication. It should be pointed out that no calculation of the production rate of the Cs_2SnCl_6 NCs derived from the Cs_2SnCl_6 powders was performed, since it is very difficult, if not impossible, to dry the oily ligands on the NCs and to determine the production rate of the Cs_2SnCl_6 NCs. Different volume ratios (VRs) of OA to OAm (40 μL to 10 μL , 30 μL to 20 μL , 25 μL to 25 μL , 20 μL to 30 μL , and 10 μL to 40 μL) were used in the preparation of the mixtures. All the preparation and synthesis processes were performed under ambient conditions. The as-obtained Cs_2SnCl_6 NCs in the solution emit blue light under ultraviolet (UV) light (365 nm) and do not emit light under white light (WL) (Fig. 1).

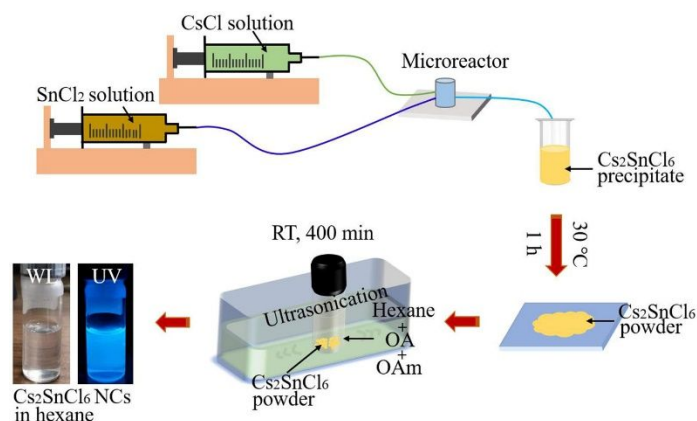


Figure 1. Schematic of the synthesis route of Cs_2SnCl_6 NCs.

2.2 Characterization

XRD (X-ray diffraction) measurements were carried out on an X-ray diffractometer (Bruker-AXS D8 Discover) with $\text{CuK}\alpha$ radiation of 1.54060 \AA in wavelength. PL measurements were performed under a UV light of 365 nm in wavelength on a Horiba Scientific Fluoromax Plus-C fluorometer, and PLQY tests were performed on a Horiba Scientific Fluoromax Plus-C fluorometer equipped with an integrated sphere. The Horiba Scientific FluorEssenceTM software was used in the PLQY calculation. UV stability tests were performed in an UV Stratalinker (model 1800) with 254-nm UV light bulbs.

PL lifetime decay measurements were performed using a DeltaHubTM high throughput time correlated single photon counting (TCSPC) controller and a NanoLED-350 pulsed excitation source (excitation wavelength $350\pm 10 \text{ nm}$). The decay curves were analysed using the Horiba Scientific decay analysis software DAS6. High-angle annular dark-field scanning transmission electron microscopy (HAADF-STEM) and high-resolution transmission electron microscopy (HRTEM) (Thermo-scientific Talos F200X operated at an accelerating voltage of 200 kV) were used to analyze the morphologies and structures of the Cs_2SnCl_6 NCs. The compositional analysis of the Cs_2SnCl_6 NCs was conducted on an energy dispersive X-ray (EDX) spectroscope (Thermo-scientific Super-X System with four windowless silicon-drift-detectors installed on a Talos F200X TEM).

3. Results and discussion

The composition and structure of the as-prepared Cs_2SnCl_6 powder was analysed by XRD. Fig. 2a shows XRD patterns (bottom) of the freshly prepared Cs_2SnCl_6 powder. It is evident that the XRD pattern matches well with the standard JCPDS card (PDF#00-007-0197), which indicates that the Cs_2SnCl_6 powder has a cubic structure with a point group of Fm-3m . This result is in good agreement with the report given by Zhang et al.²⁴ The characteristic peaks centred at 24.2° , 29.8° , 34.5° and 42.6° correspond to (220), (222), (440) and (422) crystal planes of cubic Cs_2SnCl_6 , respectively. There is a small diffractive peak centred at 32.8° , which matches with the standard JCPDS card (PDF# 00-030-0370), revealing the presence of small amount of CsSn_2Cl_5 in the Cs_2SnCl_6 powder. The CsSn_2Cl_5 was formed through the chemical reaction of Sn^{2+} with Cs^+ and Cl^- in the aqueous solution. Compared with the XRD pattern of the freshly prepared Cs_2SnCl_6 powder, the XRD pattern of the Cs_2SnCl_6 powder exposed in the air under ambient conditions for 50 days does not show any shifts of the peaks and any new peaks. The peak intensities for both the fresh powder and the one exposed in the air for 50 days remain almost the same. Note that there exists peak splitting of the XRD patterns in both the fresh and 50-day specimens. The peak splitting may be due to the lattice interpenetration, which may lead to the changes in the symmetry of cubic phase.²⁵ These results suggest good structural stability of the Cs_2SnCl_6 powder. It is worth noting that the impurity

(CsSn_2Cl_5) disappears after 50 days, which suggests inferior structural stability of CsSn_2Cl_5 compared with Cs_2SnCl_6 .

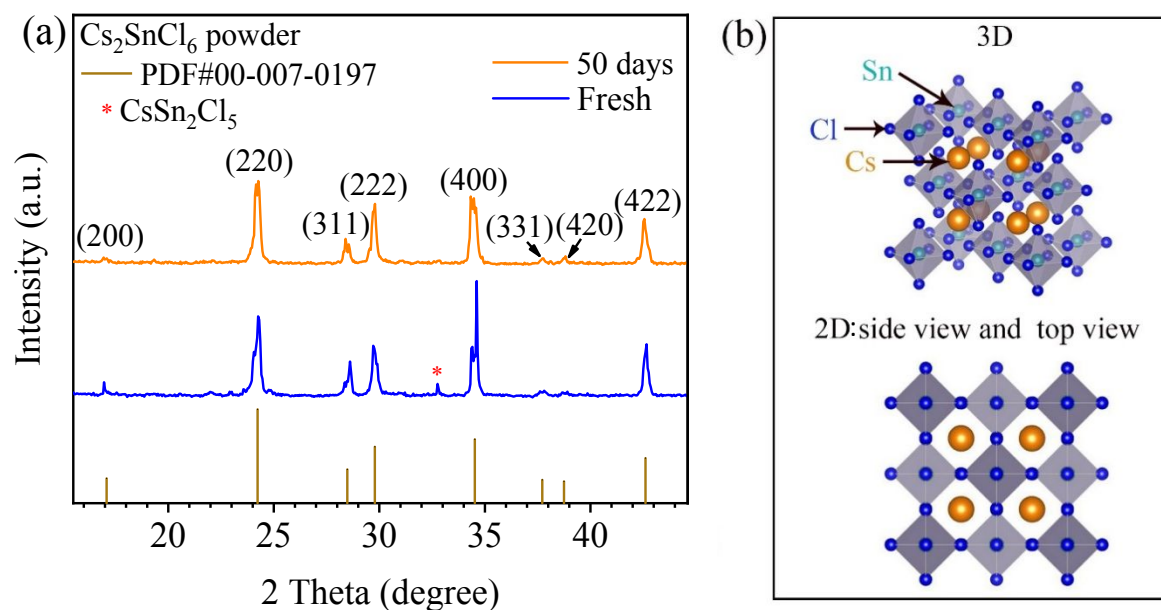


Figure 2. (a) XRD patterns of the Cs_2SnCl_6 powder, and (b) crystal structure of cubic Cs_2SnCl_6 perovskite of 3D and 2D views.

The SEM image in Fig. S2 (Supplementary Information) shows the morphology of the as-synthesized Cs_2SnCl_6 powder, which is octahedral in agreement with the report by Zhang et al.²⁶ The EDS results (Figure S3 and Table S1 in Supplementary Information) reveal that the atomic ratio of Cs:Sn:Cl is 19.79:11.30:68.92, close to the stoichiometric ratio of 2:1:6. This result further confirms that the as-prepared powder is Cs_2SnCl_6 .

The crystal structure of cubic Cs_2SnCl_6 perovskite is shown in Fig. 2b, in which the top and bottom layers illustrate 3D and 2D views, respectively. In the 3D view, the Cs_2SnCl_6 crystal contains $[\text{SnCl}_6]^{2-}$ octahedra coordinating with alkali metal cation (Cs^+). In an octahedral $[\text{SnCl}_6]^{2-}$, a Sn^{4+} is shared with six Cl^- . The crystal structure of Cs_2SnCl_6 can be considered as that a B-site cation in a double perovskite ($\text{A}_2\text{B}'\text{B}''\text{X}_6$) is replaced with a vacancy. Therefore, Cs_2SnCl_6 can be represented as $\text{A}_2\text{B}\square\text{X}_6$ and called vacancy-ordered double perovskites.²⁷ It looks like that every other $[\text{BX}_6]^{2-}$ octahedron is removed in a ABX_3 cubic perovskite.

The bottom of Fig. 2b represents 2D side (top) view of the crystal structure of cubic Cs_2SnCl_6 perovskite. For a cubic structure, the top- and side-views of the crystal structure are same. The dark and light grey squares represent the $[\text{SnCl}_6]^{2-}$ octahedra, which are not in the same plane.

The Cs_2SnCl_6 NCs were fabricated by a subsequent ultrasonication of the Cs_2SnCl_6 powder in a hexane solution consisting of OA and OAm. Fig. 3a schematically illustrates the process, in which Cs_2SnCl_6 powders of large sizes (microcrystals) are fragmented into NCs under ultrasonication. During

ultrasonication, Cs_2SnCl_6 powders of large sizes experience dynamic deformation and absorb acoustic energy. Increasing the absorbed energy causes the cracking of the powders and the crack growth through the powders, eventually leading to the breakage of the powders.²⁸ Such processes occur over and over again; consequently, small NCs are formed. Note that the ultrasonic wave-derived force on a particle is proportional to the volume of the particle.²⁹

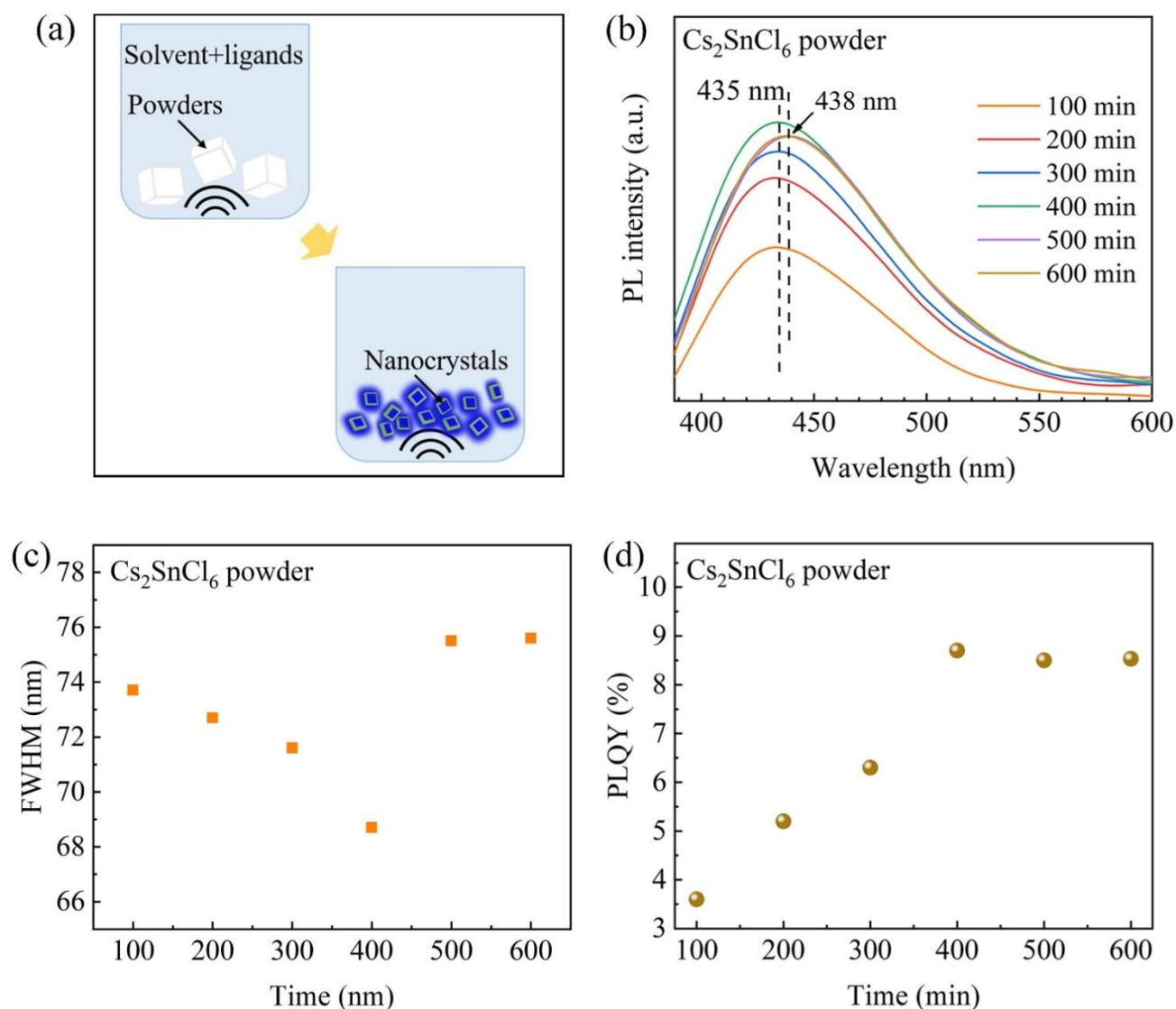


Figure 3. (a) Schematic of ultrasonication for the preparation of Cs_2SnCl_6 NCs; (b) PL spectra and (d) PLQY of the Cs_2SnCl_6 NC solution derived from the Cs_2SnCl_6 powder in a hexane solution consisting of OA and OAm (VR is 40:10) under ultrasonication for 100-600min, and (c) FWHM of (b).

Ligands (mixture of OA and OAm) play an inevitable role in the formation of NCs. The ligands wrap the formed NCs during ultrasonication to produce more and more NCs in the solution and limit the agglomeration of the NCs. OA as a capping agent on the surfaces of NCs helps to stabilize the morphology (or shape) of NCs,³⁰ and OAm is beneficial for the formation of smaller crystals.³¹ It was reported that bulk

crystals were usually formed without the use of amines when synthesizing perovskite NCs.³² Note that OAm can increase the binding between OA and NCs, which contributes to the PLQY increase of NCs, as reported by Roo et al.³³ These results suggest a synergistic effect between OA and OAm, which not only helps the formation of NCs but also enhances the optoelectronic characteristics of the NCs.

Fig. 3b shows the PL spectra (under an excitation wavelength of 365 nm (Fig. S4, Supplementary Information)) of the Cs₂SnCl₆ NC solutions derived from the Cs₂SnCl₆ powder with a VR of 40:10 for different ultrasonication times of 100, 200, 300, 400, 500 and 600 min, respectively. It is evident that the PL intensity centred at 435 nm increases with increasing the ultrasonication time. The FWHM of the PL spectra in Fig. 3b is shown in Fig. 3c. For the ultrasonication time in a range of 100-600 min, the FWHM of the PL spectra of the Cs₂SnCl₆ NC solutions decreases from ~73.7 to ~68.7 nm with increasing the ultrasonication time from 100 to 400 min and then increases to ~75.5 and ~75.6 nm for the ultrasonication times of 500 and 600 min, respectively. The PL results are qualitatively in good accord with the PLQY trend shown in Fig. 3d. The PLQYs of the Cs₂SnCl₆ NCs solutions are 3.6, 5.2, 6.3, and 8.7% after the solutions with Cs₂SnCl₆ powders were ultrasonicated for 100, 200, 300, and 400 min, respectively. It should be noted that no blue shift or red shift was observed for the Cs₂SnCl₆ NCs in the solution after a series of ultrasonication in a period of 100-400 min, indicating comparable sizes of NCs in the solution. The increase of the PL-peak intensity and PLQY can be attributed to the increase of the concentration of Cs₂SnCl₆ NCs in the solution. If strong photon scattering due to a high concentration of NCs is negligible, more photons are emitted from the same excitation volume in the solution, leading to the increase of PL-peak intensity. The PLQY, η , can be calculated as¹³

$$\eta = \frac{\int I_{sample} - \int I_{black}}{N_{ex}} \quad \text{with} \quad N_{ex} = \int I_{ex,black} - \int I_{ex,sample} \quad (1)$$

where N_{ex} is the number of photons emitted from the excitation light source, I_{sample} and I_{black} are the emission (PL) intensity of the specimen and black sample, respectively, and $I_{ex,black}$ and $I_{ex,sample}$ are the emission intensity of the excitation light from specimen and black sample, respectively. For a measurement system, I_{black} and N_{ex} are constant. Equation (1) indicates the increase of PLQY (η) with the increase of the PL intensity of specimen (I_{sample}). Therefore, a higher concentration of NCs leads to a higher PLQY.

Comparing the PL spectra of the NC solution ultrasonicated for 500 and 600 min with the PL spectrum for the same NC solution ultrasonicated for 400 min, we note slight decreases in the PL intensity and a small red shift of 3 nm of the PL peak. Correspondingly, the PLQY of the NC solution decreases to 8.5% (500 min) and 8.53% (600 min). Such results suggests that the photon scattering in the NC solution

ultrasonicated for 500 and 600 min is likely not negligible. The red shift might be caused by the size effect (size increase) of the NCs due to agglomeration.

The absorbance spectra of the Cs_2SnCl_6 NC solutions prepared from the Cs_2SnCl_6 powder (VR is 40:10) under ultrasonication for 100-400 min are presented in Fig. S5 (Supplementary Information). In consistence with the PL intensity shown in Fig. 3b, the absorbance of the NC solutions increases with the increase of the ultrasonication time to 400 min, indicating the increase in the concentration of Cs_2SnCl_6 NCs in the solution. Note that the increase of PLQY can also be attributed to quantum size effect when average NC size become smaller.³⁴

To examine if there exists the quantum size effect, we performed HAADF-STEM imaging of the sizes of the Cs_2SnCl_6 NCs. Fig. 4a shows a HAADF-STEM image of the 400 min-ultrasonicated Cs_2SnCl_6 NCs, as represented by the white spots. Fig. 4b shows the size distribution of the Cs_2SnCl_6 NCs with an average size of ~ 2.49 nm, which is comparable to an average size of ~ 2.52 nm for the 100 min-ultrasonicated NCs (Fig. S6a-b, Supplementary Information). This result suggests that there is no significant size effect on the PLQY enhancement and supports the result that no shift of the PL peak is observed in Fig. 3b for the ultrasonication time up to 400 min. It also indicates that the passivation of ligands (OA and OAm) has an insignificant effect on the PLQY enhancement of the NCs because the concentration of surface defects of a NC is mainly dependent on the NC size.

The lattice fringe determined from a typical HRTEM image (inset, upper corner in Fig. 4a) is 3.71 \AA , which corresponds to (220) crystal plane and is in accord with the corresponding SAED (selected area electron diffraction) pattern of cubic Cs_2SnCl_6 (inset, lower corner in Fig. 4a. For an enlarged view, see Fig. S6c in Supplementary Information). These results are consistent with the standard JCPDS card (PDF#00-007-0197). The EDX mappings in Fig. 4c-e reveal uniform distributions of the elements for the Cs_2SnCl_6 NCs shown in Fig. 4a. Note that only a few colour spots representing the elements are present on the mappings because a short duration time was used in the EDX mappings. The NCs are so sensitive to the electron beam that a long-time exposure to the electron beam causes the decomposition of the NCs.

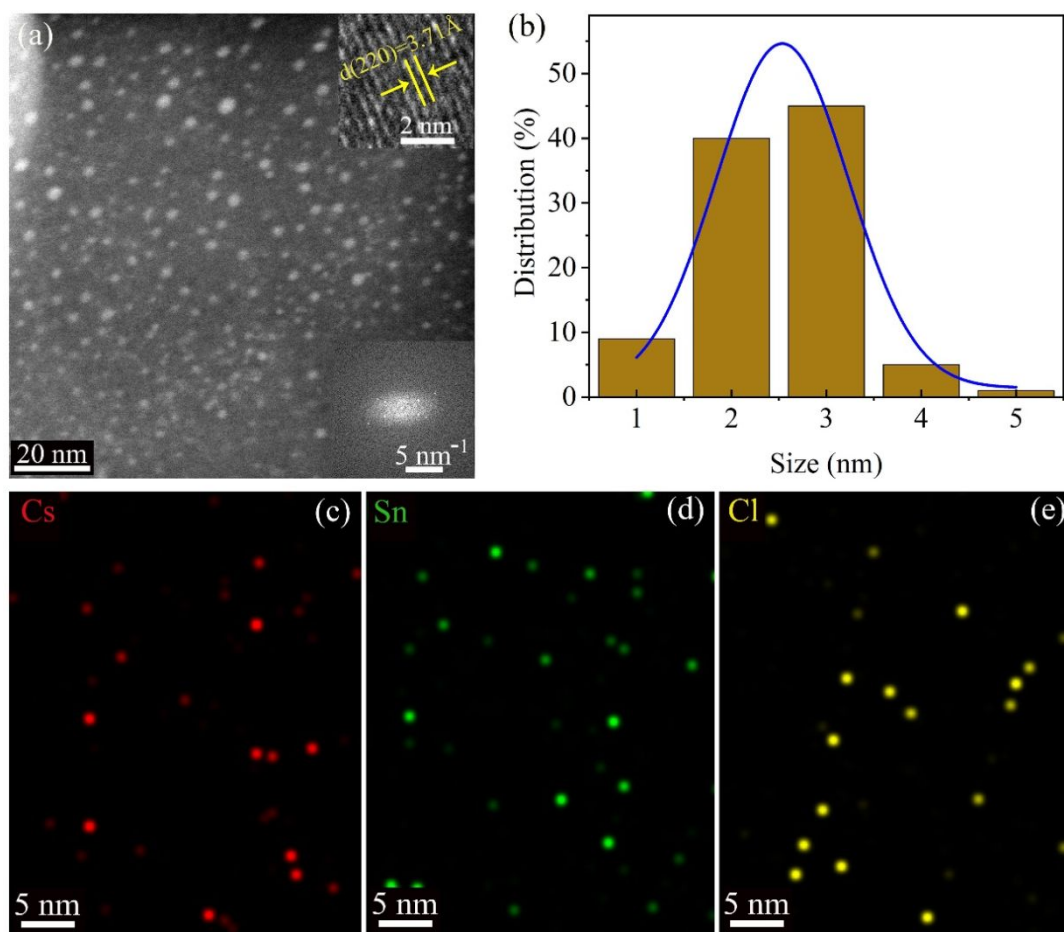


Figure 4. (a) A HAADF-STEM image of Cs_2SnCl_6 NCs prepared with 40:10 of the volume ratio of OA to OAm after an ultrasonication of 400 min. Inset: a HRTEM image (upper right) and a SAED pattern (lower right), (b) size distribution of the Cs_2SnCl_6 NCs in (a), and (c-e) elemental mapping of the Cs_2SnCl_6 NCs in (a).

We used different volume ratios of OA to OAm in the synthesis of Cs_2SnCl_6 NCs in order to examine the synergistic effect of OA and OAm on the optical characteristics of the Cs_2SnCl_6 NCs. Fig. 5a depicts the PL spectra of the Cs_2SnCl_6 NC solutions with five different volume ratios. The Cs_2SnCl_6 NC solution with a VR of 40 μL :10 μL possesses the highest PL-peak intensity with a peak wavelength of 435 nm. Decreasing the volume ratio of OA to OAm from 40 μL :10 μL to 10 μL :40 μL causes the decrease of the PL-peak intensity; the PL peak exhibits a slight red shift to 436 nm for the VR of 30 μL :20 μL and then a blue shift to 429 nm for the VR of 10 μL :40 μL . The variations of the PL-peak intensity and wavelength with the volume ratio of OA to OAm demonstrate the synergistic effect of OA and OAm on the PL characteristics of the prepared Cs_2SnCl_6 NCs. Note that the solutions prepared with only OA or OAm in hexane did not emit any light under a UV light (365 nm).

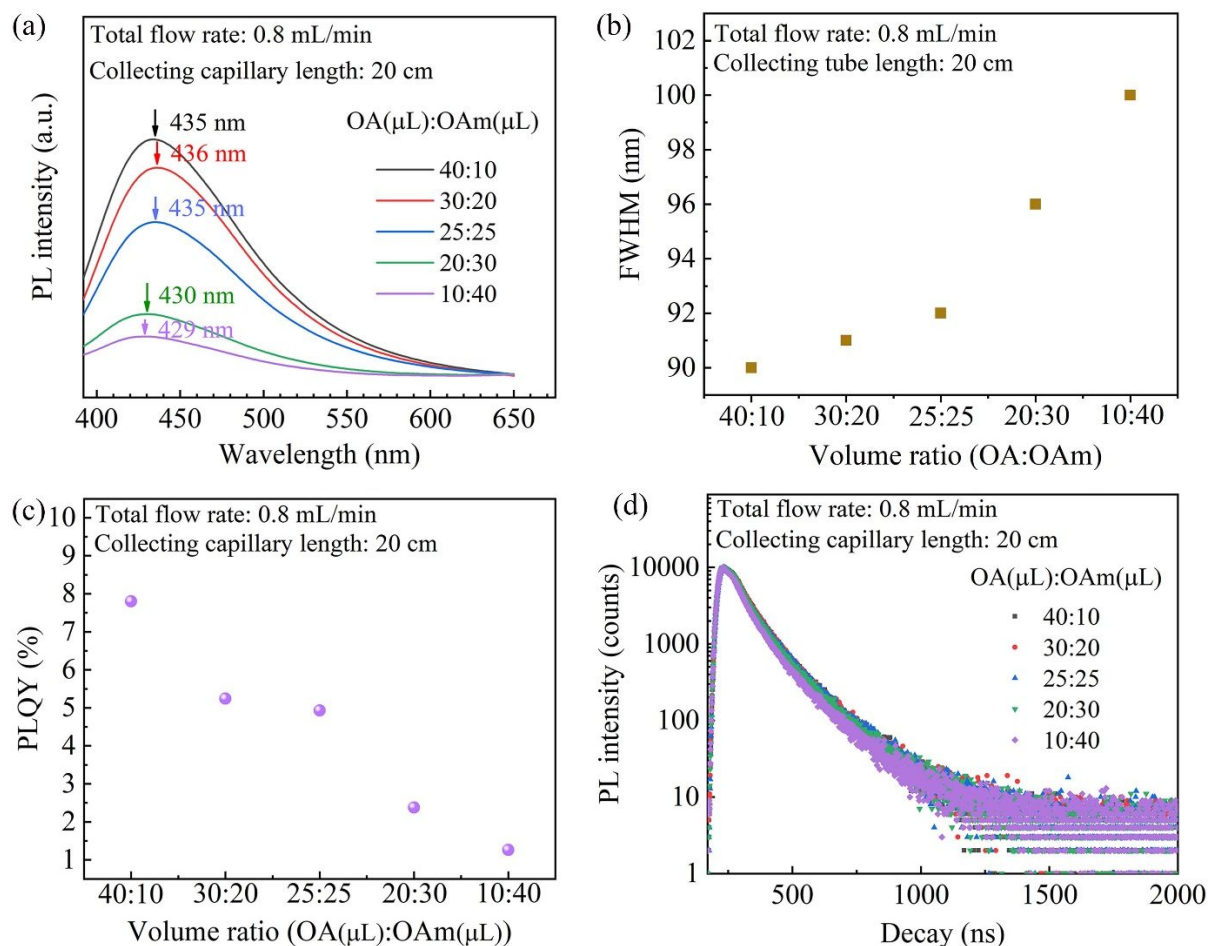


Figure 5. (a) PL, (c) PLQY, and (d) lifetime of the Cs_2SnCl_6 NC solutions prepared with different volume ratios of OA to OAm; (b) FWHM of (a).

The absorbance spectra of the prepared Cs_2SnCl_6 NCs with different volume ratios (Fig. S7, Supplementary Information) also exhibit similar characteristics to the PL spectra. Fig. 5b presents the corresponding FWHM of the PL spectra in Fig. 5a. The FWHM increases from ~90.0 to ~100.0 nm with the decrease of the VR of OA to OAm from 40:10 to 10:40.

Fig. 5c shows the decrease of the PLQY of the prepared Cs_2SnCl_6 NCs with decreasing the volume ratio of OA to OAm, which is consistent with the decreasing trend of the PL-peak intensity with decreasing the volume ratio of OA to OAm. Decreasing the volume ratio of OA to OAm from 40 μL :10 μL to 10 μL :40 μL causes the decrease of the PLQY of the Cs_2SnCl_6 NC solutions from 7.8% to 1.3%. The carrier lifetime of the Cs_2SnCl_6 NC solution also exhibits a declining trend, as revealed by the carrier lifetime decay curves in Fig. 5d.

We calculated the carrier lifetimes of the Cs_2SnCl_6 NCs by fitting the decay curves with a double exponential function as³⁵

$$I_{\text{pl}} = A_1 \exp(-t/\tau_1) + A_2 \exp(-t/\tau_2) \text{ with } A_1 + A_2 = 1 \quad (2)$$

where I_{pl} , τ_1 and τ_2 are the PL-peak intensity and the carrier lifetimes of short-lived interactive state (nonradiative recombination at surface) and long-lived non-interactive state (radiative recombination at core) of the Cs_2SnCl_6 NCs, respectively. A_1 and A_2 are the fractional contributions of the short-lived interactive state and long-lived non-interactive state, respectively.³⁵⁻⁴¹ Table 1 summarizes the numerical results of τ_1 and τ_2 . Both the τ_1 and τ_2 decrease with the decrease of the volume ratio of OA to OAm. This can be attributed to the loss of the passivation of OA on the surfaces of NCs, which leads to an increase of surface trap density.

Table 1. Lifetimes of the Cs_2SnCl_6 NCs prepared with different volume ratios of OA to OAm in hexane

	Volume ratio				
	40 μL :10 μL	30 μL :20 μL	25 μL :25 μL	20 μL :30 μL	10 μL :40 μL
τ_1 (ns)	3.52	3.51	3.40	3.13	2.93
τ_2 (ns)	8.18	8.16	8.08	7.77	7.49

The wavelength effects of the excitation light on the PL characteristics of the Cs_2SnCl_6 NCs were investigated using lights of 290, 315, 340, and 365 nm in excitation wavelengths. The study was focused on the Cs_2SnCl_6 NC solution with 40:10 in the volume ratio of OA to OAm, since this Cs_2SnCl_6 NC solution exhibited the best PL performance. Fig. S8 (Supplementary Information) depicts the PL spectra of the Cs_2SnCl_6 NC solution with and without the excitation lights of 290, 315, 340, and 365 nm in excitation wavelengths. Note that the intensities of the excitation lights are so strong that the intensities of the emitting lights are not clearly observable, as shown in Fig. S8a with both the excitation and emitting lights. Fig. S8b presents the PL spectra of the Cs_2SnCl_6 NC solution without the excitation lights. It is evident that there are four emitting lights of 581, 631, 423 and 435 nm excited by the lights of 290, 315, 340, and 365 nm, respectively. The mechanism for such behavior is unclear. The presence of the emitting lights of different emission wavelengths (423 and 435 nm) might be due to the bandgap change of the Cs_2SnCl_6 NCs associated with the difference in the electron concentrations⁴² under various excitation wavelengths. It is interesting to note that there are two strong emissions centred at 581 and 631 nm with narrow FWHMs under the excitation lights of 315 and 290 nm, respectively, which can be likely attributed to an artifact of the measurements.

The PL characteristics of the Cs_2SnCl_6 NCs from the Cs_2SnCl_6 powders prepared with different total flow rates and the lengths of capillary tube were also examined to illustrate the possible effects of the total flow rate and the length of capillary tube. Fig. S9a-b (Supplementary Information) presents the PL spectra of the Cs_2SnCl_6 NC solutions from the Cs_2SnCl_6 powders prepared with different VRs and two different capillary lengths of 20 cm and 60 cm under a total flow rate of 0.4 mL/min. Similar to the PL characteristics of the Cs_2SnCl_6 NC solution from the Cs_2SnCl_6 powders prepared under a total flow rate of 0.8 mL/min

and the capillary length of 20 cm, the PL peaks of the NC solutions prepared with a total flow rate of 0.4 mL/min and the capillary length of 20 cm exhibit a slight red shift of 2 nm first and a subsequent blue shift to 429 nm when the volume ratio of OA to OAm was decreased from 40:10 to 10:40; the PL peaks of the NC solutions prepared with a total flow rate of 0.4 mL/min and the capillary length of 60 cm exhibit a red shift first from 435 nm to 439 nm and then a blue shift from 439 nm to 429 nm when the volume ratio of OA to OAm was decreased from 40:10 to 10:40. These results are in good agreement with the corresponding PLQY results. As shown in Fig. S10a-b (Supplementary Information), decreasing the volume ratio of OA to OAM from 40:10 to 10:40 causes the decreases of the PLQYs from 6.17% to 0.6% for the Cs₂SnCl₆ NC solutions from the Cs₂SnCl₆ powders made with the total flow rate of 0.4 mL/min and the capillary length of 20 cm and 6.15% to 0.83% for the Cs₂SnCl₆ NC solutions from the Cs₂SnCl₆ powders made with the total flow rate of 0.4 mL/min and the capillary length of 60 cm. Fig. S11a-b (Supplementary Information) presents the lifetime decay curves of the Cs₂SnCl₆ NC solutions with different volume ratios of OA to OAm, which were prepared from the Cs₂SnCl₆ powders synthesized under a total flow rate of 0.4 mL/min for two capillary lengths of 20 cm and 60 cm, respectively. The carrier lifetimes of the Cs₂SnCl₆ NCs are summarized in Tables S2-3 (Supplementary Information). According to the results, we can conclude that changing the total flow rate and the capillary length has insignificant effects on the PL, PLQY and carrier lifetime of the prepared Cs₂SnCl₆ NCs.

Define $(\lambda, \vartheta_{\beta}, \vartheta_{\rho}) = [(\eta, \tau_1, \tau_2)|_{VR=40:10} - (\eta, \tau_1, \tau_2)|_{VR=10:40}] / (\eta, \tau_1, \tau_2)|_{VR=10:40}$, in which the subscript represents the volume ratio of OA to OAm. Using the data in Figs. 5c and S9, the ratio of λ is found to be 5, 9 and 6 for the Cs₂SnCl₆ NC solutions made from the Cs₂SnCl₆ powders prepared with the total flow rates of 0.8 mL/min (the capillary length of 20 cm), 0.4 mL/min (the capillary length of 20 cm) and 0.4 mL/min (the capillary length of 60 cm), respectively. However, the ratios of ϑ_{β} and ϑ_{ρ} are less than one. Such behavior is likely attributed to the difference in the radiative recombination rates of the Cs₂SnCl₆ NC solutions. It is known that both the lifetime and PLQY of NCs are determined by radiative recombination rate (η_{rad}) and non-radiative recombination rate ($\eta_{\text{non-rad}}$). The average lifetime (τ_{ave}) of NCs is calculated as⁴³

$$\tau_{\text{ave}} = (A_1\tau_1^2 + A_2\tau_2^2) / (A_1\tau_1 + A_2\tau_2) = 1 / (\eta_{\text{rad}} + \eta_{\text{non-rad}}) \quad (3)$$

and the PLQY is calculated as^{43, 44}

$$\eta = \eta_{\text{rad}} / (\eta_{\text{rad}} + \eta_{\text{non-rad}}) \quad (4)$$

which gives

$$\eta = \eta_{\text{rad}} (A_1\tau_1^2 + A_2\tau_2^2) / (A_1\tau_1 + A_2\tau_2) \quad (5)$$

with $\eta_{\text{rad}} = r_{\text{coe}} \cdot p \cdot n$ (r_{coe} , p and n are the recombination coefficient, hole concentration and electron concentration, respectively).⁴⁵ Thus, the PLQY of NCs is determined by the radiative recombination rate and the lifetimes. With λ in a range of 5 to 9 and $\tilde{\tau}_1$ and $\tilde{\tau}_2$ less than 1, it can be concluded that η_{rad} is larger than 1. This result reveals the important role of the volume ratio of OA to OAm in the radiative recombination rate associated with the recombination coefficient, hole concentration and electron concentration of the Cs_2SnCl_6 NCs.

The blue shift of the PL-peak wavelength of the Cs_2SnCl_6 NCs (Fig. 5a and S9) can be attributed to the increase in the amount of OAm. Excessive OAm molecules can shear Cs_2SnCl_6 NCs into smaller ones due to the -NH- in OAm,³⁰ as illustrated in Fig. 6. Under the action of OA and OAm, smaller NCs of ~ 2.02 nm in average size (Fig. S12a-b, Supplementary Information) emit blue light of shorter wavelengths due to quantum size effect.^{46, 47}

The surface chemistry of the Cs_2SnCl_6 NC solutions with various volume ratios of OA to OAm is analysed on a Thermo Nicolet IS50 FT-IR spectrometer with a diamond attenuated total reflectance plate. As shown in Fig. S13 (Supplementary Information), the peak intensity for the N-H bond centred at 1552 cm^{-1} ⁴⁸ increases with the decrease of the volume ratio of OA to OAm (40:10 to 10:40), indicating an increase in the interaction between OAm and the NCs. This is in good accord with the increasing shear effect with the increase of OAm, as discussed above. The decreases in the peak intensities of the C=O bond centred at 1712 cm^{-1} ⁴⁹ and C-O bond centred at 953 cm^{-1} ⁵⁰ are in line with the decrease of the volume ratio of OA to OAm from 40:10 to 10:40, which indicates the weaker interaction between OA and NCs.

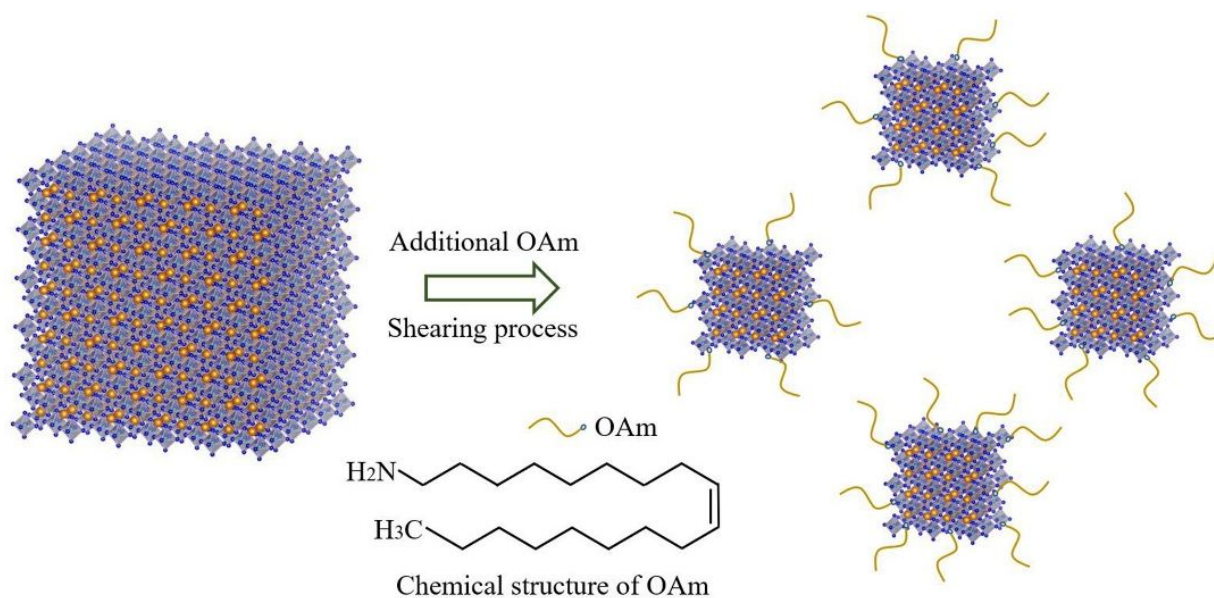


Figure 6. Schematic for the shearing of Cs_2SnCl_6 NCs by OAm.

It should be noted that the PL-peak intensity and PLQY (Fig. 5c) of the Cs_2SnCl_6 NCs exhibit the decreasing trend with decreasing the NC sizes instead of the increasing trend associated with the quantum size effect.⁴⁷ This is highly due to that increasing the amount of OAm in the NC solution increases the scattering of emitted photons and blocks the light emitted from the solution. Another possible reason for the decreasing of the PLQY with the increase of OAm is that decreasing OA (Fig. S11) reduces the passivation function in controlling the surface defects of NCs,³⁰ which causes an ascending nonradiative recombination of holes and electrons. This is in accord with the lifetime results shown in Figs. 5d and S8 and Tables 1, S2 and S3.

To further investigate the role of individual ligand in controlling the PL characteristics of the Cs_2SnCl_6 NCs, the volume (50 μL) of OA was maintained constant and the volume ratio of OA to OAm was varied from 50:10, 50:20, ..., to 50:80 in the preparation of the Cs_2SnCl_6 NC solutions in 5 mL hexane. The as-obtained PL spectra are shown in Fig. S14a in Supplementary Information. The PL peak for the NC solution with the volume ratio of 50:10 is centred at 437 nm; the PL peak experiences red shifts of 1 and 4 nm for the volume ratios of 50:20 and 50:30, respectively, and blue shift with the decrease of the volume ratio from 50:40 to 50:80. The red shift of the PL peak is highly likely due to the change of the interface stress/energy⁵¹ between ligands and NCs caused by the increase in the OAm volume. Further increasing the OAm volume increases the contribution of the shear effect, leading to the blue shift. Fig. S14b shows the variation of the PLQY of the Cs_2SnCl_6 NC solutions with the volume ratio of OA to OAm with 50 μL OA, which follows a similar trend to the PL intensity, similar to the results shown in Fig. 3b and d.

The volume effects on the PL characteristics of the Cs_2SnCl_6 NC solutions were also evaluated with the volume ratios of OA to OAm of 40:10, 50:20, 60:30, 70:40 and 80:50 in 5 mL hexane. As shown in Fig. S15 (Supplementary Information), the PL-peak intensity (Fig. S15a) and the corresponding PLQY (Fig. S15b) decrease with the decrease of the volume ratio of OA and OAm from 50:20 to 80:50. The PL-peak wavelength fluctuates between 440 nm and 438 nm, suggesting that increasing the amount of OA in the specimen preparation can hinder the shift of the PL peak.

Considering that the Cs_2SnCl_6 NC solution prepared with 40:10 of the volume ratio of OA to OAm exhibited the highest PLQY, we examined the long-term optical stability of the Cs_2SnCl_6 NCs in the Cs_2SnCl_6 NC solution, as shown in Fig. 7. Over a period of 60 days, the PLQY fluctuates in a range of 7.03 to 8.25 (Fig. 7a) and the PL-peak wavelength fluctuates in a range of 434 to 436 nm without significant red or blue shift (Fig. 7b). These results support that the prepared Cs_2SnCl_6 NCs possess sound and stable optical properties.

Considering that the Cs_2SnCl_6 NC solution prepared with 40:10 of the volume ratio of OA to OAm exhibited the highest PLQY, we examined the long-term optical stability of the Cs_2SnCl_6 NCs in the

Cs_2SnCl_6 NC solution, as shown in Fig. 7. Over a period of 60 days, the PLQY fluctuates in a range of 7.03 to 8.25 (Fig. 7a) and the PL-peak wavelength fluctuates in a range of 434 to 436 nm without significant red or blue shift (Fig. 7b). These results support that the prepared Cs_2SnCl_6 NCs possess sound and stable optical properties.

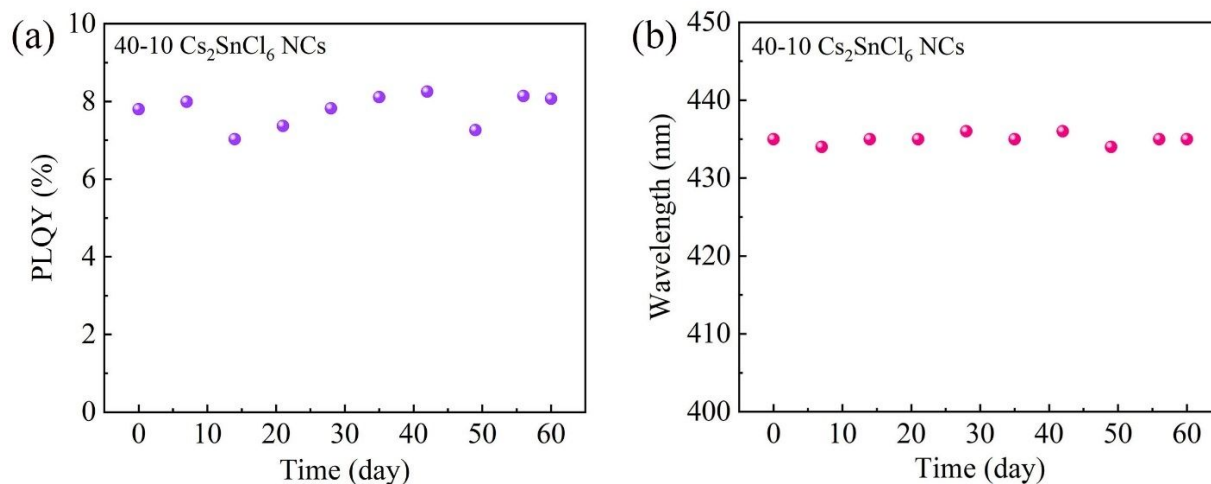


Figure 7. Optical stability of the Cs_2SnCl_6 NC solution over a period of 60 days: (a) PLQY, and (b) PL-peak wavelength.

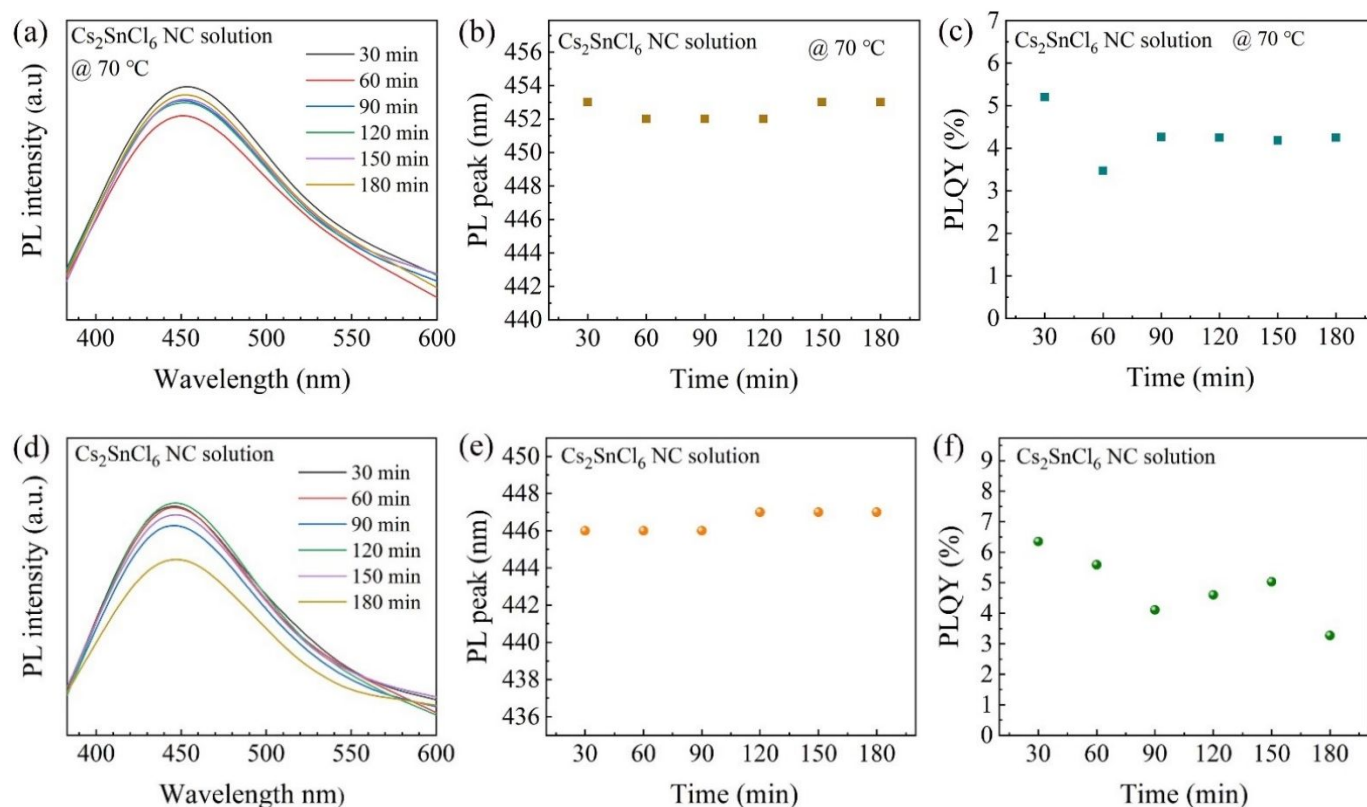


Figure 8. (a-c) Thermal stability and UV stability (d-f) of the Cs_2SnCl_6 NC solution over a period of 180 min: (a) PL spectra of the Cs_2SnCl_6 NC solution heated at 70 °C, (b) PL-peak wavelength of the PL spectra

in (a), (c) PLQY of the Cs_2SnCl_6 NC solution in (a), (d) PL spectra of the Cs_2SnCl_6 NC solution under UV light (254 nm in wavelength, 3 mW/cm² in irradiation rate), (e) PL-peak wavelength of the spectra in (d), and (f) PLQY of the Cs_2SnCl_6 NC solution in (d).

The thermal stability (Fig. 8a-c) and UV stability (Fig. 8d-f) of the Cs_2SnCl_6 NC solution prepared with 40:10 of the volume ratio of OA to OAm were evaluated. Fig. 8a shows the PL spectra of the Cs_2SnCl_6 NC solution heated at 70 °C over a period of 180 min. The PL peaks fluctuate in a range of 452-453 nm (Fig. 8b); the PL-peak intensity decreases with increasing the heating time to 60 min, and then increases with increasing the heating time from 60 to 180 min to a nearly constant intensity. The variation of the PLQY with the heating time (Fig. 8c) exhibits a nearly similar trend to the PL-peak intensity.

The PL spectra of the Cs_2SnCl_6 NC solution under a UV light (254 nm in wavelength, 3 mW/cm² in irradiation rate) over a period of 180 min is displayed in Fig. 8d. The emission peaks centre at 446 nm for first 90 min and at 447 nm from 120 to 180 min (Fig. 8e). This result suggests that the UV stability of the Cs_2SnCl_6 NC solution is better than the thermal stability in the emission wavelength. The PLQY of the Cs_2SnCl_6 NC solution decreases from 6.35% (UV for 30 min) to 3.27% (UV for 180 min) (Fig. 8d) similar to the UV effect on the PL intensity.

We prepared three different Cs_2SnCl_6 NC solutions from the same Cs_2SnCl_6 powders with three conventionally used solvents (dichloromethane, isopropyl alcohol (IPA) and toluene in 5 mL with 40:10 of the volume ratio of OA to OAm). Table S4 in Supplementary Information summaries the PL characteristics of the prepared Cs_2SnCl_6 NC solutions. The Cs_2SnCl_6 NC solutions have the highest PLQY of 7.96% and the lowest PLQY (0.46%) with the IPA and toluene as the solvent, respectively. The PL-peak wavelengths are 442, 446 and 450 nm for the Cs_2SnCl_6 NC solutions with IPA, dichloromethane and toluene as the solvent, respectively. Note that IPA has the highest polarity (0.546)⁵² and toluene has the lowest polarity of 0.099.⁵² However, it cannot be concluded that the higher the polarity, the larger is the PLQY, since the PLQY of the Cs_2SnCl_6 NC solution prepared with hexane of 0.009 in polarity as the solvent is larger than the Cs_2SnCl_6 NC solution with IPA as the solvent. It is the combinational effects of solvent and ligands that determine the PL characteristics, including PL-peak wavelength and PLQY, of the Cs_2SnCl_6 NC solution.

As a green route to synthesize Cs_2SnCl_6 NCs, we used polydimethylsiloxane (PDMS) as a non-toxic ligand to synthesize Cs_2SnCl_6 NCs. Specifically, silicone elastomer base with mass in a range of 0.01-0.05 g was used as ligand to synthesize Cs_2SnCl_6 NCs in hexane. The PLQY of the Cs_2SnCl_6 NC solutions increases from 0.53 to 4.23% with increasing the amount of silicone elastomer base from 0.01 to 0.04 g. Further increasing the amount of the silicone elastomer base to 0.05 g caused the drop of the PLQY to 2.86%, as shown in Table S5 in Supplementary Information. This result indicates silicone elastomer base can be used as a green ligand in the synthesis of Cs_2SnCl_6 NCs. We also used silicone elastomer curing

agent and the mixture of silicone elastomer curing agent and silicone elastomer base to evaluate if these materials can be used as ligands to improve the PLQY of Cs_2SnCl_6 NC solutions. However, no PLQY was detectable for the prepared NC solutions. The possible reason is that silicone elastomer curing agent is not a capping agent that can wrap the NCs and disperse stable NCs in the solution. Also, silicone elastomer curing agent crosslinks with silicone elastomer base.^{53, 54} In this case, silicone elastomer curing agent will prevent the silicone elastomer base as a role of ligand contributing to the formation of Cs_2SnCl_6 NCs from Cs_2SnCl_6 powder. This might be the cause that no PLQY of the NC solutions was detectable when the mixture of silicone elastomer curing agent and silicone elastomer base was used as a possible ligand. Another possible reason for this undetected PLQY is the polarity of hexane (Table S4, Supplementary Information), which may have a negative effect on the formation of Cs_2SnCl_6 NCs with silicone elastomer curing agent.

Table 2 summarizes the synthesis method and the optical characteristics of blue-emitting Sn-based lead-free NCs available in the literature. It is evident that the synthesis method used in this work is much simple and the optical characteristics of the prepared Cs_2SnCl_6 NCs are superior or comparable to those reported in the literature except the Bi-doped Cs_2SnCl_6 NCs reported by Tan et al.¹³ However, Tan et al.¹³ used solvothermal process, which requires a high synthesis temperature near 200 °C and limits the amount of NCs prepared per batch.

More importantly, the Cs_2SnCl_6 NCs in hexane exhibited a remarkable stability over 60 days, much longer than the one by other methods. The superior stability of the Cs_2SnCl_6 NCs is likely due to the stronger Sn-Cl bond than some other perovskite family materials, such as CsSnCl_3 .⁵⁵ In general, the stability of a cubic Cs_2SnCl_6 will be improved when the size of the crystal decreases in a specific range. This is due to a smaller surface energy of (100) surface, leading to a significant stability for cubic crystal.⁵⁶ In contrast to the Cs_2SnCl_6 NCs prepared by the method presented in this work, the one prepared by hot injection experiences a thermal quenching process from a high temperature (around 150 °C) to the ice point in a mixture of ice and water. There are more structural defects presented in the NCs, which influence the associated optical characteristics.^{57, 58} That is to say, the Cs_2SnCl_6 NCs prepared by hot injection possess is at non-equilibrium state and can experience structural relaxation at room temperature, leading to the changes in optical characteristics over a time period. Note that structural defects are also the cause of optical instability for perovskite materials.⁵⁹⁻⁶¹ Figure S16 (Supplementary Information) presents optical images of fresh and 60-day' Cs_2SnCl_6 NC solutions, which show no precipitates presented in the Cs_2SnCl_6 NC solution after 60 days. The superior stability can likely be due to the smaller size and less defects of the Cs_2SnCl_6 NCs than the ones prepared by hot injection.

Table 2. Comparison of blue-emitted Sn-based lead-free NCs reported in literature and this work

Materials (LFPe NCs)	Synthesis method	Wavelength (nm)	PLQY (%)	Stability	Ref.
CsSnCl ₃	HI	~480	0.14	14 days	12
CsSnCl ₃	HI	475	0.17	-	62
Bi-doped Cs ₂ SnCl ₆	Solvothermal	455	78.9	2.9% decrease of PL intensity in water in 120 min	13
Cs ₂ SnCl ₆	HI	438	4.37	<20 s (irradiation)	63
Sb-doped Cs ₂ SnCl ₆	HI	438/615	8.25	>20 s (irradiation)	63
Cs ₂ SnCl ₆	HI	444	-	-	64
Cs ₂ SnCl ₆	Microfluidics & ultrasonication	435	13.4 (Table S6, Supplementary Information)	60 days (in air)	This work

4. Conclusions

We have demonstrated the feasibility to synthesize LFHP Cs₂SnCl₆ microcrystals in a large scale on a microfluidic platform using green aqueous solution at room temperature. Placing the LFHP Cs₂SnCl₆ microcrystals in a hexane solution, we have produced blue-emitting Cs₂SnCl₆ NCs by a ultrasonication process. The experimental results reveal that the PLQY of the prepared Cs₂SnCl₆ NCs increases with increasing the ultrasonication time due to the increase of the NC concentration in the solution. Decreasing the volume ratio of oleic acid to oleylamine causes the decrease of the PLQY of the Cs₂SnCl₆ NC solution and the shift of the PL-peak wavelength first to a large wavelength and then to small wavelengths. The PLQY decrease is attributed to the increase of the non-radiative recombination of charge carriers caused by the passivation loss of OA on the surfaces of NCs. The blue shift is due to the excessive -NH- shearing effect, which reduces the sizes of large NCs. The long-term stability tests indicate that the Cs₂SnCl₆ NC in the solution have an excellent optical stability in air over a period of 60 days without significant changes in the PLQY and PL-peak wavelength. This study opens a green-route approach for a large-scale fabrication of LFHP NCs, such as Cs₂SnX₆ (Cl, Br and I), and is expected to extend to other lead-free NCs.

Conflicts of interest

There are no conflicts to declare.

Acknowledgements

FY is grateful for the support by the NSF through the grant CMMI-1854554, monitored by Drs. Khershed Cooper and Thomas Francis Kuech, and CBET- 2018411 monitored by Dr. Nora F Savage.

Notes and references

1. Y. Wei, Z. Cheng and J. Lin, *Chemical Society Reviews*, 2019, **48**, 310-350.
2. G. W. Kim and A. Petrozza, *Advanced Energy Materials*, 2020, **10**, 2001959.
3. H. Huang, M. I. Bodnarchuk, S. V. Kershaw, M. V. Kovalenko and A. L. Rogach, *ACS Energy Letters*, 2017, **2**, 2071-2083.
4. C. Bi, Z. Yao, X. Sun, X. Wei, J. Wang and J. Tian, *Advanced Materials*, 2021, **33**, 2006722.
5. M. Sulaman, S. Yang, Z. Zhang, A. Imran, A. Bukhtiar, Z. Ge, Y. Tang, Y. Jiang, L. Tang and B. Zou, *Materials Today Physics*, 2022, **27**, 100829.
6. Y. Chen, J. Yin, Q. Wei, C. Wang, X. Wang, H. Ren, S. F. Yu, O. M. Bakr, O. F. Mohammed and M. Li, *Nature Photonics*, 2022, 1-6.
7. Z. Shi, J. Guo, Y. Chen, Q. Li, Y. Pan, H. Zhang, Y. Xia and W. Huang, *Advanced Materials*, 2017, **29**, 1605005.
8. Y. Yan, T. Pullerits, K. Zheng and Z. Liang, *ACS Energy Letters*, 2020, **5**, 2052-2086.
9. Y. Wang, J. Tu, T. Li, C. Tao, X. Deng and Z. Li, *Journal of Materials Chemistry A*, 2019, **7**, 7683-7690.
10. J.-M. Heo, H. Cho, S.-C. Lee, M.-H. Park, J. S. Kim, H. Kim, J. Park, Y.-H. Kim, H. J. Yun and E. Yoon, *ACS Energy Letters*, 2022, **7**, 2807-2815.
11. F. Yuan, X. Zheng, A. Johnston, Y.-K. Wang, C. Zhou, Y. Dong, B. Chen, H. Chen, J. Z. Fan and G. Sharma, *Science Advances*, 2020, **6**, eabb0253.
12. T. C. Jellicoe, J. M. Richter, H. F. Glass, M. Tabachnyk, R. Brady, S. E. Dutton, A. Rao, R. H. Friend, D. Credgington and N. C. Greenham, *Journal of the American Chemical Society*, 2016, **138**, 2941-2944.
13. Z. Tan, J. Li, C. Zhang, Z. Li, Q. Hu, Z. Xiao, T. Kamiya, H. Hosono, G. Niu and E. Lifshitz, *Advanced Functional Materials*, 2018, **28**, 1801131.
14. R. Cheng, Z. B. Liang, L. Zhu, H. Li, Y. Zhang, C. F. Wang and S. Chen, *Angewandte Chemie*, 2022, e202204371.
15. X. Tang and F. Yang, *Lab on a Chip*, 2022, **22**, 2832-2843.
16. V. Sebastian, *Nanoscale*, 2022, **14**, 4411-4447.
17. S. Marre and K. F. Jensen, *Chemical Society Reviews*, 2010, **39**, 1183-1202.
18. R. W. Epps, K. C. Felton, C. W. Coley and M. Abolhasani, *Lab on a Chip*, 2017, **17**, 4040-4047.
19. S. Kubendhiran, Z. Bao, K. Dave and R.-S. Liu, *ACS Applied Nano Materials*, 2019, **2**, 1773-1790.

20. I. Lignos, S. Stavrakis, G. Nedelcu, L. Protesescu, A. J. deMello and M. V. Kovalenko, *Nano Letters*, 2016, **16**, 1869-1877.
21. Z. Bao, J.-W. Luo, Y.-S. Wang, T.-C. Hu, S.-Y. Tsai, Y.-T. Tsai, H.-C. Wang, F.-H. Chen, Y.-C. Lee and T.-L. Tsai, *Chemical Engineering Journal*, 2021, **426**, 130849.
22. Y. Geng, J. Guo, H. Wang, S. D. Ling, Z. Chen, S. Chen and J. Xu, *Small*, 2022, **18**, 2200740.
23. Y. Geng, J. Guo, S. D. Ling, X. Wu, H. Liu, Z. Chen, S. Chen and J. Xu, *Science China Materials*, 2022, 1-9.
24. H. Zhang, L. Zhu, J. Cheng, L. Chen, C. Liu and S. Yuan, *Materials*, 2019, **12**, 1501.
25. J. Hafizovic, M. Bjørgen, U. Olsbye, P. D. Dietzel, S. Bordiga, C. Prestipino, C. Lamberti and K. P. Lillerud, *Journal of the American Chemical Society*, 2007, **129**, 3612-3620.
26. H. Zhang, L. Zhu, J. Cheng, L. Chen, C. Liu and S. Yuan, *Crystals*, 2019, **9**, 258.
27. A. E. Maughan, A. M. Ganose, M. M. Bordelon, E. M. Miller, D. O. Scanlon and J. R. Neilson, *Journal of the American Chemical Society*, 2016, **138**, 8453-8464.
28. F. Yu, *Particulate Science and Technology*, 2021, **39**, 91-100.
29. S. M. Woodside, B. D. Bowen and J. M. Piret, *AIChE journal*, 1997, **43**, 1727-1736.
30. H. Xiao, Y. Wei, P. Dang, S. Liang, Z. Cheng, G. Li and J. Lin, *Journal of Materials Chemistry C*, 2020, **8**, 9968-9974.
31. Y. Zhang, T. D. Siegler, C. J. Thomas, M. K. Abney, T. Shah, A. De Gorostiza, R. M. Greene and B. A. Korgel, *Chemistry of Materials*, 2020, **32**, 5410-5423.
32. S. E. Creutz, E. N. Crites, M. C. De Siena and D. R. Gamelin, *Nano Letters*, 2018, **18**, 1118-1123.
33. J. De Roo, M. Ibáñez, P. Geiregat, G. Nedelcu, W. Walravens, J. Maes, J. C. Martins, I. Van Driessche, M. V. Kovalenko and Z. Hens, *ACS Nano*, 2016, **10**, 2071-2081.
34. X. Tang, N. L. Kothalawala, Y. Zhang, D. Qian, D. Y. Kim and F. Yang, *Chemical Engineering Journal*, 2021, **425**, 131456.
35. Z. Wu, M. Jiang, Z. Liu, A. Jamshaid, L. K. Ono and Y. Qi, *Advanced Energy Materials*, 2020, **10**, 1903696.
36. D. Shi, V. Adinolfi, R. Comin, M. Yuan, E. Alarousu, A. Buin, Y. Chen, S. Hoogland, A. Rothenberger and K. Katsiev, *Science*, 2015, **347**, 519-522.
37. B. G. Yacobi and D. B. Holt, *Cathodoluminescence microscopy of inorganic solids*, Springer Science & Business Media, 2013.
38. J. T. DuBose and P. V. Kamat, *The Journal of Physical Chemistry C*, 2020, **124**, 12990-12998.
39. Y. J. Yoon, Y. S. Shin, C. B. Park, J. G. Son, J. W. Kim, H. S. Kim, W. Lee, J. Heo, G.-H. Kim and J. Y. Kim, *Nanoscale*, 2020, **12**, 21695-21702.

40. J. Li, Z. Han, Y. Gu, D. Yu, J. Liu, D. Hu, X. Xu and H. Zeng, *Advanced Functional Materials*, 2021, **31**, 2008684.
41. Y. Liu, Z. Yang and S. Liu, *Advanced Science*, 2018, **5**, 1700471.
42. E. N. Economou, *The physics of solids: essentials and beyond*, Springer Science & Business Media, 2010.
43. B. Shu, Y. Chang, J. Zhang, X. Cheng and D. Yu, *Nano Research*, 2021, **14**, 3352-3357.
44. I. G. Scheblykin, *Advanced Energy Materials*, 2020, **10**, 2001724.
45. S. M. Sze, Y. Li and K. K. Ng, *Physics of semiconductor devices*, John Wiley & sons, 2021.
46. E. Hanamura, in *Confined Electrons and Photons*, Springer, 1995, pp. 831-837.
47. L. Protesescu, S. Yakunin, M. I. Bodnarchuk, F. Krieg, R. Caputo, C. H. Hendon, R. X. Yang, A. Walsh and M. V. Kovalenko, *Nano Letters*, 2015, **15**, 3692-3696.
48. R. Tareb, M. Bernardeau, C. Amiel and J.-P. Vernoux, *Microbiology Letters*, 2017, **364**, fnw298.
49. K. Fahmy, F. Jäger, M. Beck, T. A. Zvyaga, T. P. Sakmar and F. Siebert, *Proceedings of the National Academy of Sciences*, 1993, **90**, 10206-10210.
50. J. Huberty and R. Madix, *Surface Science*, 1996, **360**, 144-156.
51. F. Yang, *Physics Letters A*, 2022, **428**, 127931.
52. C. Reichardt and T. Welton, *Solvents and solvent effects in organic chemistry*, John Wiley & Sons, 2010.
53. J. Schweitzer, S. Merad, G. Schrodj, F. Bally-Le Gall and L. Vonna, *Journal of Chemical Education*, 2019, **96**, 1472-1478.
54. Z. Wang, A. A. Volinsky and N. D. Gallant, *Journal of Applied Polymer Science*, 2014, **131**.
55. Z. Xiao, H. Lei, X. Zhang, Y. Zhou, H. Hosono and T. Kamiya, *Bulletin of the Chemical Society of Japan*, 2015, **88**, 1250-1255.
56. A. S. Barnard and P. Zapol, *The Journal of Chemical Physics*, 2004, **121**, 4276-4283.
57. M. A. Reshchikov, *physica status solidi (a)*, 2021, **218**, 2000101.
58. I. Buyanova, W. Chen, G. Pozina, B. Monemar, W.-X. Ni and G. Hansson, *Applied Physics Letters*, 1997, **71**, 3676-3678.
59. S. Chen, X. Wen, S. Huang, F. Huang, Y. B. Cheng, M. Green and A. Ho-Baillie, *Solar Rrl*, 2017, **1**, 1600001.
60. A. Hassan, Z. Wang, Y. H. Ahn, M. Azam, A. A. Khan, U. Farooq, M. Zubair and Y. Cao, *Nano Energy*, 2022, 107579.
61. B. w. Park and S. I. Seok, *Advanced Materials*, 2019, **31**, 1805337.

62. C. Kang, H. Rao, Y. Fang, J. Zeng, Z. Pan and X. Zhong, *Angewandte Chemie*, 2021, **133**, 670-675.
63. Y. Jing, Y. Liu, J. Zhao and Z. Xia, *The Journal of Physical Chemistry Letters*, 2019, **10**, 7439-7444.
64. A. Veronese, M. Patrini, D. Bajoni, C. Ciarrocchi, P. Quadrelli and L. Malavasi, *Frontiers in Chemistry*, 2020, **8**, 35.